Disease Expression in Usher Syndrome Caused by *VLGR1* Gene Mutation (*USH2C*) and Comparison with *USH2A* Phenotype

Sharon B. Schwartz,[1] *Tomas S. Aleman,*[1] *Artur V. Cideciyan,*[1] *Elizabeth A. M. Windsor,*[1] *Alexander Sumaroka,*[1] *Alejandro J. Roman,*[1] *Tej Rane,*[1] *Elaine E. Smilko,*[1] *Jean Bennett,*[1] *Edwin M. Stone,*[2] *William J. Kimberling,*[3] *Xue-Zhong Liu,*[4] *and Samuel G. Jacobson*[1]

Purpose. To investigate the retinal disease expression in *USH2C*, the subtype of Usher syndrome type 2 recently shown to be caused by mutation in the *VLGR1* gene, and compare results with those from *USH2A*, a more common cause of Usher syndrome.

Methods. Three siblings with *USH2C* and 14 patients with *USH2A* were studied. Visual function was measured by kinetic perimetry, static chromatic perimetry, and electroretinography (ERG). Central retinal microstructure was studied with optical coherence tomography (OCT).

Results. The siblings with *VLGR1* mutation showed abnormal photoreceptor-mediated function in all retinal regions, and there was greater rod than cone dysfunction. *USH2A* had a wider spectrum of disease expression and included patients with normal function in some retinal regions. When abnormalities were detected, there was more rod than cone dysfunction. Retinal microstructure in both *USH2C* and *USH2A* shared the abnormality of loss of outer nuclear layer thickness. Central retinal structure in both genotypes was complicated by cystic macular lesions. A coincidental finding in an *USH2C* patient was that oral intake of antihistamines was associated with temporary resolution of the macular cystic change.

Conclusions. *USH2C* and *USH2A* manifest photoreceptor disease with rod- and cone-mediated visual losses and thinning of the outer nuclear layer. An orderly progression through disease stages was estimated from cross-sectional and limited longitudinal data. Intrafamilial and interfamilial variation in retinal severity in *USH2A*, however, suggests that genetic or nongenetic modifiers may be involved in the disease expression.

(*Invest Ophthalmol Vis Sci.* 2005;46:734–743) DOI:10.1167/iovs.04-1136

Usher syndrome (USH) is an autosomal recessive group of diseases characterized by retinal degeneration and hearing loss. Three subtypes are clinically distinguishable, mainly by degree of hearing dysfunction and the presence or absence of vestibular abnormality (reviewed in Refs. 1–3). In patients with USH type II (USH2), the most common subtype,[4,5] the congenital hearing loss is relatively mild at low frequencies and severe at high frequencies and can be either stable or progressive.[6,7] Patients with USH2 do not have vestibular dysfunction, in contrast to the profound hearing loss with vestibular abnormality in USH1. USH3 has progressive hearing loss with variable vestibular abnormalities.[8]

Approximately 70% of USH2 is caused by mutations in *USH2A* (MIM 608400) on 1q41,[3,9] but molecular heterogeneity has been demonstrated.[10–13] A genome scan in 12 USH2 families who were unlinked to 1q41 and *USH2B* (MIM 276905) markers localized a third USH2 gene to the long arm of chromosome 5.[14] More recently, the *USH2C*-associated gene at this locus was identified to be very large G protein-coupled receptor-1 (*VLGR1*; MIM 605472).[15]

Details of retinal phenotype in *USH2C* have not been described. We report results of psychophysical, electrophysiological, and retinal imaging studies in affected members of a family with *USH2C*[10,14] and draw comparisons by using similar analyses in a group of patients with *USH2A* mutations.

Materials and Methods

Subjects

Patients with USH, representing 11 families, underwent clinical ocular examinations and visual function studies. Molecular results for the *USH2C* family are published (family 1848 in Refs. 14,15). Other patients with *USH2A* were identified.[13] All subjects gave informed consent, institutional review board approval was obtained, and the tenets of the Declaration of Helsinki were followed.

Visual Function Studies

Psychophysics. Kinetic perimetry was performed with two targets (V-4e and I-4e). Dark- and light-adapted threshold chromatic perimetry was performed with a modified automated perimeter to determine rod and L/M (long/middle wavelength) cone function. Techniques, methods of data analysis, and normal results have been described.[16,17]

Electroretinography. Full field electroretinograms (ERGs) were performed with a standard protocol. Details of the methods and normal data have been published.[17–19]

Optical Coherence Tomography. Cross-sectional images of the central retina were obtained with commercially available optical

From the [1]Department of Ophthalmology, Scheie Eye Institute, University of Pennsylvania, Philadelphia, Pennsylvania; the [2]Department of Ophthalmology, Howard Hughes Medical Institute, University of Iowa Hospitals and Clinics, Iowa City, Iowa; the [3]Usher Syndrome Center, Boys Town National Research Hospital, Omaha, Nebraska; and the [4]Department of Otolaryngology, University of Miami, Miami, Florida.

Supported by National Eye Institute Grants EY13385 and EY13729; the Foundation Fighting Blindness; Macula Vision Research Foundation; Macular Disease Foundation; Research to Prevent Blindness; the Mackall Trust; and the F. M. Kirby Foundation.

Submitted for publication September 23, 2004; revised November 11, 2004; accepted November 12, 2004.

Disclosure: **S.B. Schwartz**, None; **T.S. Aleman**, None; **A.V. Cideciyan**, None; **E.A.M. Windsor**, None; **A. Sumaroka**, None; **A.J. Roman**, None; **T. Rane**, None; **E.E. Smilko**, None; **J. Bennett**, None; **E.M. Stone**, None; **W.J. Kimberling**, None; **X.-Z. Liu**, None; **S.G. Jacobson**, None

The publication costs of this article were defrayed in part by page charge payment. This article must therefore be marked "*advertisement*" in accordance with 18 U.S.C. §1734 solely to indicate this fact.

Corresponding author: Samuel G. Jacobson, Scheie Eye Institute, University of Pennsylvania, 51 North 39th Street, Philadelphia, PA 19104; jacobsos@mail.med.upenn.edu.

TABLE 1. Clinical Characteristics of the *USH2C* and *USH2A* Patients

Family (Mutation), Patient	Age at First Visit (y)/Gender	Visual Acuity (RE-LE)*	Refraction†	Kinetic Visual Field Extent (V-4e/I-4e)‡	Electroretinograms		
					Rod b-Wave Amplitude§	Cone Flicker	
						Amplitude§	Timing
USH2C (*VLGR1*)							
Family 1 (6901C→T/8716insAACA)							
P1	40/F	20/20	−0.50	78/3	ND	4	Delay
P5	33/F	20/20	−0.75	76/1	ND	8	Delay
P6	27/F	20/25–20/30	+0.50	7/5	ND	8	Delay
USH2A‖							
Family 2 (2299delG/2299delG)							
P1	26/M	20/25–20/30	−2.50	9/<1	ND	ND	ND
P4	17/F	20/20	−0.25	93/53	N	N	N
P5	17/F	20/20	Plano	99/19	ND	21	Delay
Family 3 (2299delG)							
P1	18/M	20/20	−0.50	89/<1	ND	9	Delay
Family 4 (2299delG/1214delA)							
P1	29/M	20/25	−1.50	15/<1	ND	ND	ND
Family 5 (2299delG)							
P1	39/F	20/20	−1.00	94/<1	ND	7	Delay
Family 6 (2299delG/921insCAGC)							
P1	45/F	20/40	−3.75	16/<1	ND	ND	ND
Family 7 (1550G→C/1550G→C)							
P1	31/F	20/50	Plano	24/3	ND	ND	ND
P2	29/F	20/60–20/50	−3.50	94/6	ND	3	Delay
Family 8 (2299delG)							
P1	56/F	20/30–20/40	−0.50	1/<1	np	np	np
P2	52/M	20/60–20/50	+0.50	<1/ND	ND	ND	ND
Family 9 (2299delG)							
P1	44/M	20/40–20/50	−2.00	<1/<1	np	np	np
Family 10 (2299delG)							
P1	38/F	20/25	−0.50	61/<1	ND	ND	ND
Family 11 (1679delC)							
P1	21/F	20/25	−4.00	75/<1	ND	ND	ND

N, normal; np, not performed; ND, not detectable.

* Best corrected visual acuity; similar in the two eyes unless specified.

† Spherical equivalent; average of both eyes.

‡ Average of both eyes, expressed as a percentage of normal mean for V-4e or I-4e target; 2 SD below mean equals 90%.[17]

§ Expressed as percent of mean normal amplitude, if <2 SD of normal.[19]

‖ One allele identified only in some families.

coherence tomography (OCT) instruments (OCT1 and OCT3; Carl Zeiss Meditec, Dublin, CA), according to described methods.[18,20,21] Scans were 4.5 mm long. Each scan, formed by a series of longitudinal reflectivity profiles (LRPs), was analyzed with custom-developed computer programs.[18,21–24] Retinal thickness measurements were made at the fovea and at a perifoveal temporal retinal locus. Outer nuclear layer thickness was quantified at the perifoveal locus. These measurements were based on the distance between previously defined features on averaged LRPs.[21–23]

RESULTS

Phenotype of *USH2C*

The *USH2C* family (Table 1, family 1) had four affected siblings (Fig. 1A). The causative compound heterozygous mutations in *VLGR1* have been identified as Q2301X (6901C→T) and I2906FS (8716insAACA).[15] Table 1 gives clinical characteristics of three affected family members at their first visit. Audiometric evaluations available in the siblings (P1 at age 42 years, P5 at age 39, and P6 at age 20) showed bilateral hearing impairment with a downsloping configuration: there was moderate-to-severe loss at low frequencies and severe-to-profound loss at higher frequencies.

Retinal Dysfunction. P6, P5, and P1 (at ages 27, 33, and 40 years, respectively) showed a similar pattern of retinal dysfunction by ERG (Fig. 1B). There were no detectable rod b-waves to a dim blue flash of light in the dark-adapted state. The maximal response to a white flash of light, dark-adapted, had reduced a- and b-wave amplitudes. Cone ERGs (to 1- or 29-Hz stimuli) were reduced in amplitude and delayed in timing. Rod and cone perimetry was performed at the same ages. Dark-adapted perimetry, displayed as maps of rod sensitivity loss, showed that P6 retained a central island of rod-mediated function. Light-adapted perimetry, displayed as a map of L/M cone sensitivity loss, showed the central island and a small temporal–inferior peripheral region of detectable function. P5 and P1, at older ages than P6, had more peripheral function. Shared by all patients was an extensive midperipheral region with no detectable rod- or L/M cone-mediated function (Fig. 1C).

Kinetic perimetry also illustrates the different extents of peripheral function in the siblings (Fig. 2; Table 1). P6, the youngest sibling, had a central island but no detection of the stimuli beyond the 20° isopter (Fig. 2A). Both older siblings showed midperipheral absolute scotomas and detectable peripheral function (Figs. 2B, 2C). The kinetic visual field change over a 7-year interval in P1 (ages 40–47 years) is also shown

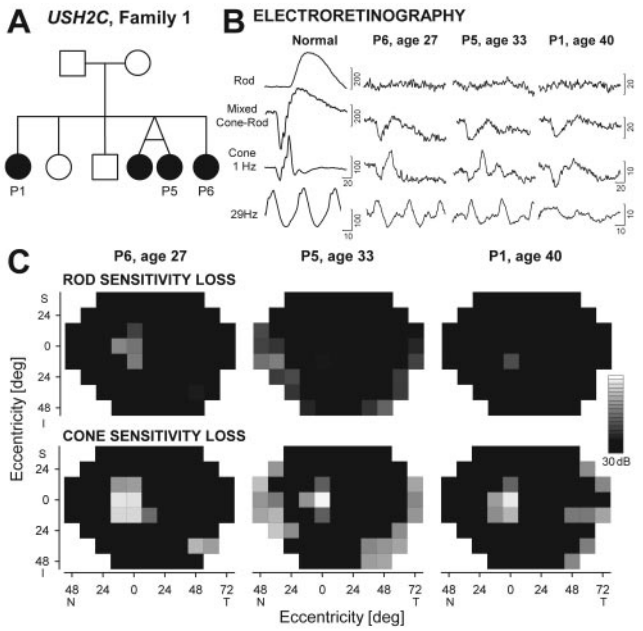

FIGURE 1. Rod and cone function in an *USH2C* family. (**A**) Pedigree. *Circles*: females; *squares*: males; *filled symbols*: affected individuals; *open symbols*: unaffected individuals. (**B**) Rod, mixed cone–rod, and cone ERGs from three siblings are compared with ERGs of a normal subject (age 35 years). Calibrations (vertical, microvolts; horizontal, milliseconds) are to the *right* and *below* the waveforms. (**C**) Static threshold perimetry results, dark-adapted (*top*) and light-adapted (*bottom*), are displayed as grayscale maps of rod and cone sensitivity loss. Scale has 16 levels of *gray*, representing 0- to 30-dB losses. The physiological blind spot is represented as a *black square* at 12° in the temporal field. N, nasal; T, temporal; I, inferior; S, superior visual field.

(Fig. 2C). The midperipheral scotomas evolved to a complete annular midperipheral defect that separated the central from the far peripheral islands.

Whereas severity of peripheral dysfunction appeared unrelated to age in this family, central rod- and cone-mediated function was more abnormal in the older siblings (Fig. 2D). P6, at age 27, retained the greatest central extent and degree of rod-mediated function. Rod sensitivity loss over most of the central island was approximately 15 to 20 dB, but there was a decline to no measurable rod function at eccentricities greater than 24°. Cone sensitivity loss in the central island of P6 (not shown) was between 5 and 10 dB at most loci, declining to unmeasurable function at 22° to 24° from fixation. P5 (age 33) and P1 (age 40) also had detectable but impaired central rod-mediated function that extended only to approximately 12° from fixation (Fig. 2D). P5 had a minimum of 15 to 20 dB rod sensitivity loss; cone sensitivity loss was approximately 5 to 10 dB. P1 had several paracentral loci with rod-mediated stimulus detection that were at least 15 dB reduced in sensitivity. Most other loci were cone-mediated with sensitivity losses of 5 to 10 dB.

Central Retinal Micropathology. A normal cross-sectional image along the horizontal meridian of the central retina (Fig. 3A) shows a foveal depression and definable laminae. Overlaid LRPs at the fovea and at a temporal perifoveal retinal locus (5.6° or 1.7 mm) highlight the differences between retinal lamination at the two locations. At the foveal locus, there was a reflection from the vitreoretinal interface, a decline in reflectivity representing the nuclear layer of cone photoreceptors, and a multipeaked high reflectivity deep in the retina, named the outer retinal–choroidal complex (ORCC).[22,23,25] The ORCC represents photoreceptor inner segments (IS) and outer segments (OS), the retinal pigment epithelium (RPE), and the anterior choroid.[20,21] At the temporal perifoveal locus, a region of high rod density,[26] there is a reflection at the vitreoretinal interface— deeper high and low reflectivities, representing synaptic and cellular layers and the ORCC (Fig. 3A).

Cross-sectional central retinal imaging through fixation from 7.5° nasal to 7.5° temporal was performed on the siblings with *USH2C* mutation. Scans are shown for both eyes of P6 and P5 at a single visit and P1 at two different ages (Figs. 3B–D). Details of the retinal laminar architecture are illustrated with LRPs overlaid at the fovea and at the temporal perifoveal locus. The scans of P6 at age 30 showed interocular asymmetry of central structure (Fig. 3B). The fovea of the right eye appeared normal but had slightly increased thickness (188 μm; normal mean ± SD, 142.5 ± 14.2 μm, n = 8). The ORCC was multipeaked similar to the normal waveform. Visual acuity was 20/25. At the temporal locus, outer nuclear layer (ONL) thickness was reduced (32 μm; normal mean ± SD, 62.9 ± 5.1 μm, n = 8). Overall retinal thickness at this locus was at the upper limits of normal (268 μm; normal mean ± SD, 243.5 ± 10.8 μm, n = 8), suggesting increased inner retinal thickness. The left eye of P6, in contrast, showed a dramatically increased foveal thickness of 472 μm with cystic changes.[27,28] The ORCC was multipeaked, and visual acuity was 20/30. At the temporal locus, the retina was also thickened (372 μm): The ONL was reduced to 32 μm but the INL was greatly expanded.

P5 at age 36 years, for comparison, had very little interocular asymmetry in microstructure (Fig. 3C). The right eye showed no major distortion of foveal architecture, but there was a slight increase in thickness (178 μm). The left eye had

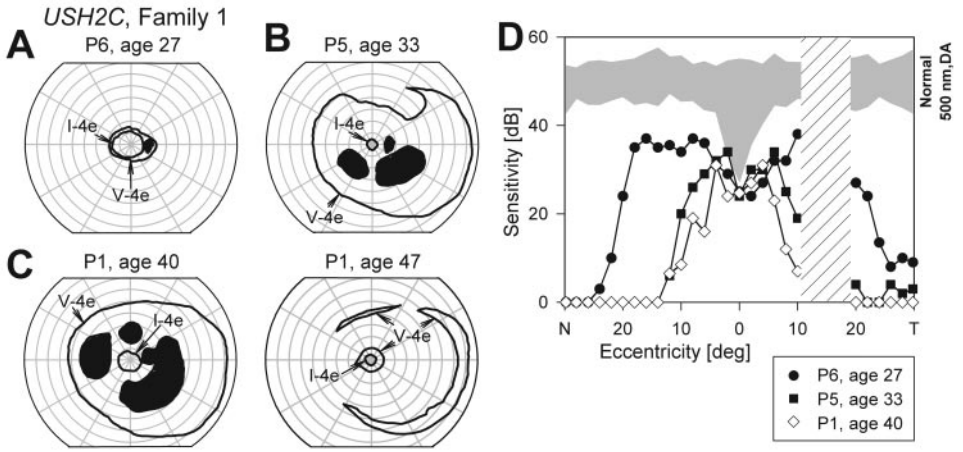

FIGURE 2. Visual field patterns and progression in *USH2C*. (**A–C**) Kinetic perimetry in P6 and P5 and in P1 at two different ages representing a 7-year interval. (**D**) Dark-adapted sensitivity profiles with a 500-nm stimulus across the central 60° of retina in the three affected members of family 1 and normal subjects (*gray*, mean ± 2 SD; n = 21, ages 15–42 years). *Hatched area*: physiological blind spot region. N, nasal; T, temporal visual field.

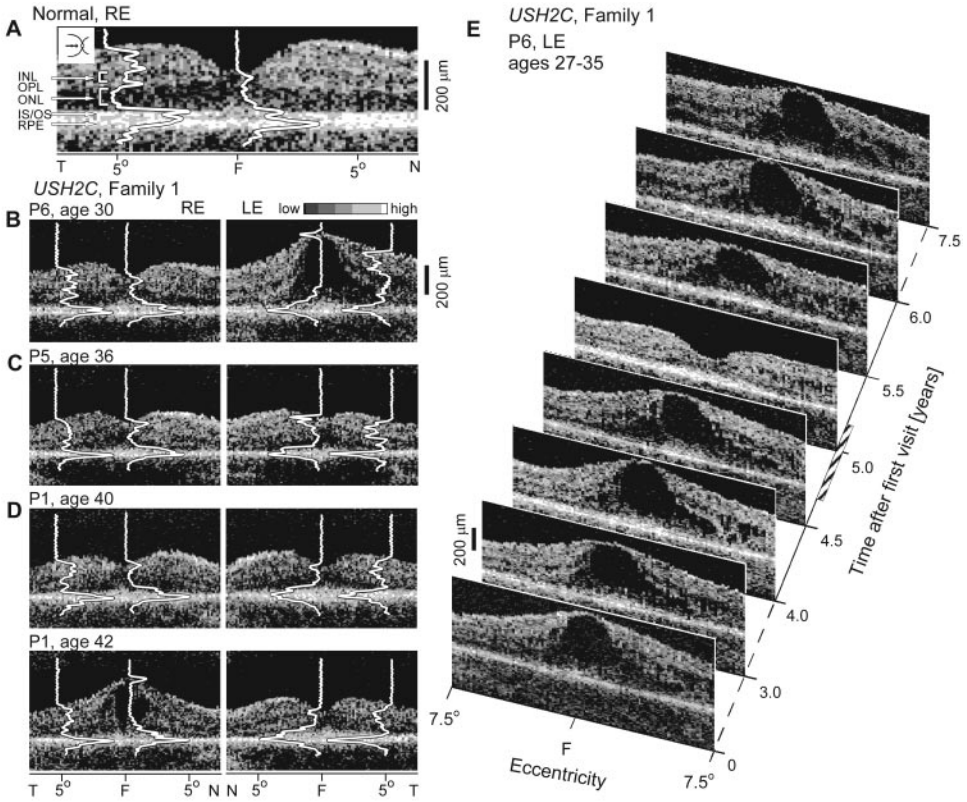

FIGURE 3. Central retinal microstructure in *USH2C*. (**A–D**) Cross-sectional retinal images obtained with OCT from the central 15° of the right eye of a 27-year-old normal subject (*inset*: scan location on fundus drawing) and both eyes of P6 (age 30), P5 (age 36), and P1 (ages 40 and 42). Images are displayed with the logarithm of reflectivity mapped to a grayscale. LRPs, averaged from 1° sections, are superimposed on the images at (or near, so as not to obscure micropathology) two locations: the fovea and at 5.6° (1.7 mm) in the temporal retina. F, fovea; N, nasal; T, temporal retina; INL, inner nuclear layer; OPL, outer plexiform layer; ONL, outer nuclear layer; IS/OS, photoreceptor inner/outer segments; RPE, retinal pigment epithelium. (**E**) Serial cross-sectional retinal images in P6 (left eye) over a 7.5-year interval. *Hatched bar* along the time axis indicates the period of oral antihistamine use.

less of a foveal depression and slightly greater thickness (216 μm). At the temporal loci in both eyes, ONL thickness was reduced (26 μm), and the ORCC was single peaked, a feature associated with loss of IS/OS in retinal degenerations.[22,23]

Serial scans in P1, separated by 2 years, show a progression to interocular asymmetry and cystic changes in the right eye (Fig. 3D). At age 40 years, foveal thickness of the right eye was normal (152 μm), but it had increased to 380 μm at age 42. The foveal ORCC was multipeaked on both visits; visual acuities were 20/20 at age 40 and 20/25 at age 42. The temporal retinal locus of the right eye was similar on the two visits with reduced ONL (24 μm). The ORCC at age 40 retained an early component attributable to the IS/OS, but at age 42 it was single peaked. Foveal thickness of the left eye was 146 and 144 μm at the two ages. Visual acuities were 20/20 and 20/25. The temporal retinal locus of the left eye differed on the two visits. The multipeaked ORCC at age 40 changed to a single-peaked ORCC at age 42, and at both times, the ONL was reduced (26 and 30 μm, respectively).

Serial scans from the left eye of P6 over a 7.5-year period (Fig. 3E) showed an unexpected result. At age 27, visual acuities were 20/20 and 20/30 in right and left eyes, respectively, and there were prominent cystic changes only in the left eye that did not change remarkably over 4.5 years (time 0 to 4.5 years; time 3 years is age 30 years; Fig. 3B). The patient was taking no prescription medicines during this interval. At the age of 32 (time ~4.6 years; Fig. 3E), the patient had seasonal allergic symptoms and began taking the antihistamine cetirizine (recalled dose, 10 mg/d), which was continued for approximately 3 months. Generalized pruritus and dermatographism of unknown cause occurred, and three further antihistamines were added in an attempt by the patient, with medical guidance, to relieve the symptoms: fexofenadine at 180 mg/d, hydroxyzine at 100 mg/d in divided doses, and diphenhydramine ad libitum (25 mg). The four antihistamines were taken together for 1 month, after which time cetirizine and diphenhydramine were discontinued. For two more months, hydroxyzine and fexofenadine were continued, and the pruritus disappeared. While taking these last two medications, the patient returned for follow-up examination (elapsed time, 5 years) and reported the events of the previous few months. No visual change was noted by the patient, and visual acuities remained similar to those recorded previously. The prominent and previously persistent macular cystic changes of the left eye were no longer detectable. Hydroxyzine and fexofenadine were continued by the patient for a further month and then stopped. On a visit 4 months after cessation of all antihistamines (5.5 years), the cystic maculopathy was again evident and similar to that of previous visits. Subsequent examinations have shown no dramatic changes in this eye (times, 6.0 and 7.5 years; Fig. 3E).

Phenotype of *USH2A*

Table 1 gives clinical characteristics of 14 patients in 10 families with *USH2A* gene mutations. Audiometric evaluations were available from 10 patients and all showed bilateral hearing impairment with a downsloping configuration.

Retinal Dysfunction. For comparison with results of ERG and chromatic perimetry in *USH2C* family 1 (Fig. 1), similar studies are shown from three affected siblings in *USH2A* family 2 (Fig. 4). P4, at age 17, had ERG results (Fig. 4B) that were at the lower limit of normal.[19] Rod and cone sensitivities were normal or nearly normal in a wide extent of the central and midperipheral visual field, but there was a decline in sensitivity in the temporal field (Fig. 4C). P5 (dizygotic twin of P4), also at age 17, had pronounced abnormalities in ERGs and perimetry. Rod ERG b-waves were not detectable and the mixed cone–rod ERG a- and b-wave amplitudes were reduced. Cone ERGs to 1-Hz stimuli were within normal limits for amplitude. The 29-Hz response had two components that were both

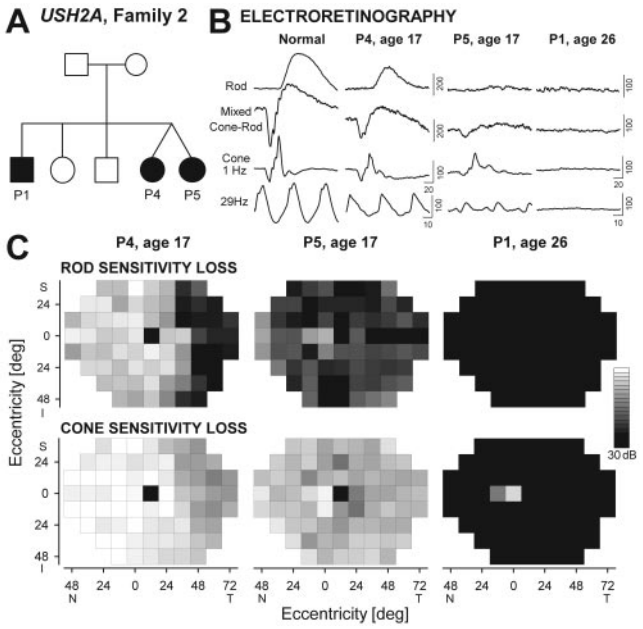

FIGURE 4. Rod and cone function in an *USH2A* family. (**A**) Pedigree. Symbols as in Figure 1. (**B**) Rod, mixed cone–rod, and cone ERGs from three siblings are compared with ERGs of a normal subject. (**C**) Static threshold perimetry results in the dark-adapted (*top*) and light-adapted (*bottom*) states are displayed as grayscale maps of rod and cone sensitivity loss. Scale has 16 levels of gray, representing 0- to 30-dB losses. N, nasal; T, temporal; I, inferior; S, superior visual fields.

reduced in amplitude (Fig. 4B). Rod sensitivities were reduced across most of the visual field outside the center (Fig. 4C). Cone sensitivities were less affected than those of the rods. P1, nearly a decade older than his siblings, had a nondetectable ERG and only a central island with impaired cone-mediated function (Figs. 4B, 4C).

Kinetic perimetry in family 2 (Fig. 5A) also showed different degrees of visual loss in the twins at age 17 years. P4 and P5 both had a normal extent of peripheral field with the V-4e test target. With the smaller target (I-4e), P4 had a reduced extent of temporal field, but P5 showed a more generalized reduction to a central island of 25° to 30° in diameter. Serial results over a 5-year interval in P5 and the results in P1, the older sibling, suggest a pattern of kinetic field progression. P5, from ages 17 to 22 years, lost substantial peripheral and paracentral field. ERG parameters over this interval (not shown) also supported a dramatic reduction in function. The mixed response lost approximately 50% amplitude and cone ERGs lost 60% to 80% amplitude. P1, at age 26 years, was limited to a small central island.

Central rod-mediated function in P4 at age 17 was at the lower limit of normal (Fig. 5B, top panel); cone sensitivity (not shown) was normal. P1 at age 26, representing a more severe disease expression, had a small central island with no measurable rod function and reduced cone sensitivity (Fig. 5B, top panel). Intermediate disease severities were suggested in the results of P5 separated by a 5-year interval (Fig. 5B, lower panel). Rod sensitivity at age 17 was nearly normal centrally but was reduced by ≥15 dB at eccentricities beyond 10° to 15°. At age 22 years, rod sensitivity was abnormally reduced at paracentral loci by 10 to 15 dB and declined to 30 dB rod sensitivity loss at eccentricities beyond 15°. Cone function was within normal limits in the central 20° on both visits. A decline in sensitivity with eccentricity was present at age 17 and was more exaggerated at age 22 (data not shown).

The patterns of results of kinetic perimetry in four representative *USH2A* patients from different families (Fig. 5C) illustrate a range of disease expression. Family 7, P2 (age 29 years), for example, retained full peripheral field extent with the V-4e target but was limited to a central island with the I-4e target. This degree of disease was greater than that in family 2, P4 and P5, at age 17. Family 10, P1 (age 38) showed midperipheral absolute scotomas and family 4, P1 (age 29) had a complete annular midperipheral scotoma separating central from peripheral islands. Serial results over 14 years in family 5, P1 documented the progression from relative to absolute midperipheral scotomas (Fig. 5E).

Central rod function measurements in three *USH2A* patients from different families (Fig. 5D) suggest a disease sequence from reduced (by 10–15 dB) but measurable rod sensitivity in the central 20° to 30° (family 3, P1), to a more limited extent (<20°) of increasingly impaired rod function (family 10, P1), to a small central cone-mediated island with no detectable rod function (family 6, P1). This proposed sequence from cross-sectional data resembles the serial dark-adapted profiles over a 14-year interval in family 5, P1 (Fig. 5F). From a nearly 40° extent of rod-mediated function with normal central rod sensitivities at age 36, there was progression to a cone-mediated central island of <20° by age 50. During this interval, cone sensitivity remained within normal limits in the very central field, but the horizontal extent of measurable function declined (data not shown).

Central Retinal Micropathology. Cross-sectional retinal imaging of the central retina was performed in seven patients with *USH2A* mutations. In family 2, the siblings P4 and P1 exemplified different degrees of abnormality in central retinal architecture (Fig. 6A). The right eye of P4 at age 17 years had a normal-appearing fovea with a thickness of 150 μm; ORCC was multi-peaked and visual acuity was 20/20. The perifoveal temporal locus was also nearly normal except for an ONL thickness of 46 μm, which was slightly reduced. The right eye of P1 at age 27 years showed an increased foveal thickness of 428 μm with a pattern of macular edema. The ORCC was multi-peaked and visual acuity was 20/25. The temporal retinal locus had discernible laminae but retinal thickness was reduced (208 μm). The ONL thickness was thinned to 16 μm, and the ORCC was single-peaked.

Serial scans in P5, separated by 3 to 4 years, illustrate a progression to overt cystic macular change in the left eye during this interval (Fig. 6B). The right eye of P5 at ages 17 and 21 had normal-appearing foveal architecture with a multipeaked ORCC; thickness in each eye was slightly increased (188 μm at 17, and 194 μm at 22 years). Visual acuity was 20/20 at ages 17 and 21. Perifoveal temporal loci showed a normal overall retinal thickness at both ages (248 and 254 μm, respectively) but ONL thickness was reduced (20–22 μm), suggesting an increase in inner retinal thickness. The left eye fovea of P5 at age 18 had slightly greater thickness at 200 μm, and at age 21 the fovea was greatly thickened at 360 μm with obvious cystic change. The ORCC at both ages was multipeaked, and visual acuity was 20/20 at age 18 and 20/25 at age 21. Perifoveal temporal loci were not remarkably different between visits. Overall retinal thickness was within normal limits at both ages (266 and 264 μm, respectively), but ONL thickness was reduced (22–24 μm) with a single-peaked ORCC; again, this suggests an increase in inner retinal thickness.

Two further examples of interocular asymmetry and micropathology related to cystic maculopathy and retinal degeneration in *USH2A* patients are shown (Figs. 6C, 6D). P1 of family 3 at age 18 years had 20/20 visual acuity in both eyes. The right eye had cystic changes and a greatly increased foveal thickness of 438 μm, whereas the left eye's foveal thickness was in-

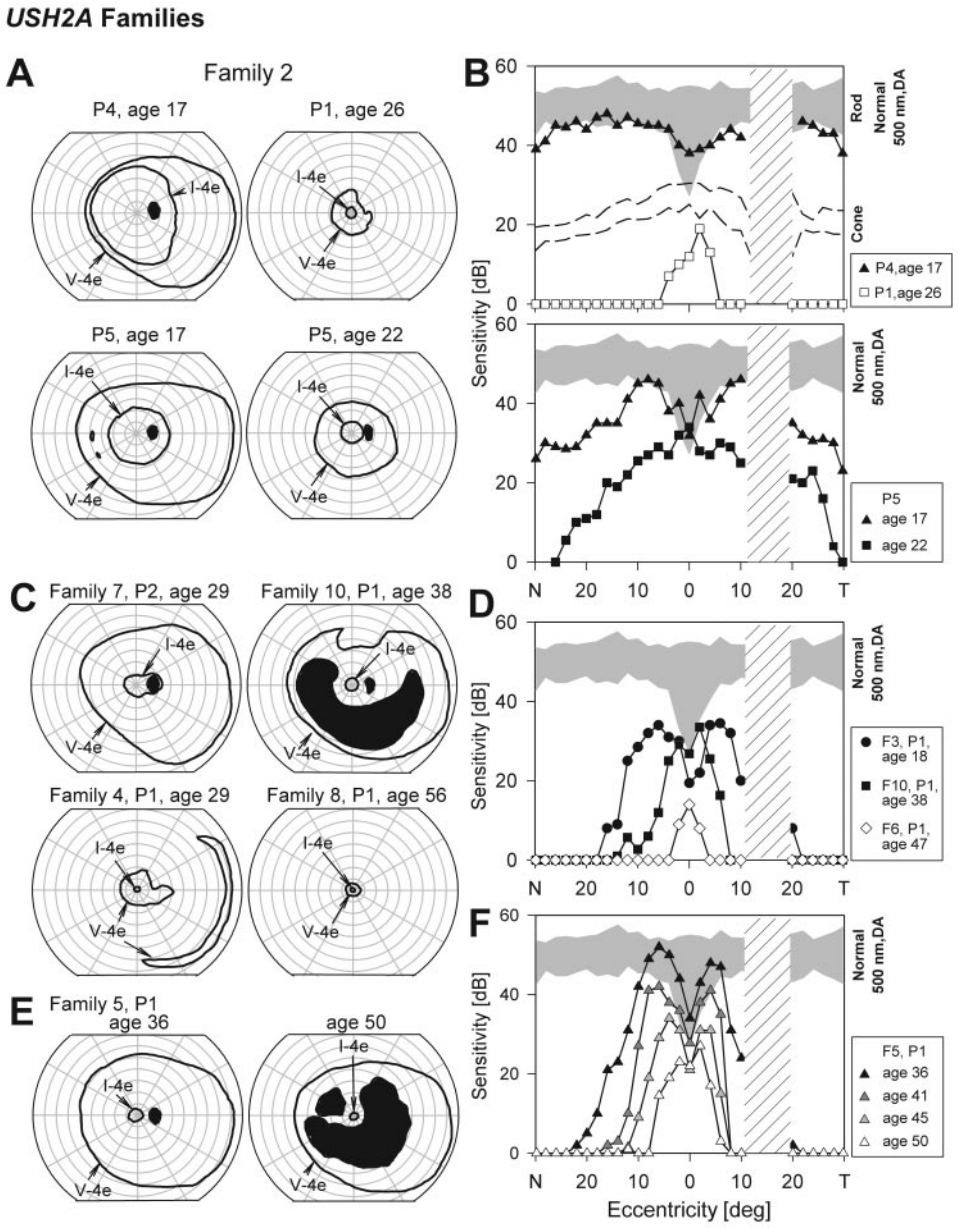

FIGURE 5. Visual field patterns and progression in *USH2A*. (**A**) Kinetic perimetry results in family 2, P4 and P1, and in P5 at two different ages representing a 5-year interval. (**B**) Dark-adapted sensitivity profiles in the three affected members of family 2 and normal subjects (*gray*, mean ± 2 SD; as in Fig. 2). Normal data (mean ± 2 SD; $n = 5$, ages 26–54 years) for this stimulus on a cone plateau is displayed for comparison with patient profiles that are cone mediated (*open symbols*). (**C**) Kinetic perimetry of patients with different degrees of visual loss. (**D**) Dark-adapted sensitivity profiles of representative patients. (**E**) Kinetic perimetry in family 5, P1 at two different ages, representing a 14-year interval. (**F**) Dark-adapted sensitivity profiles of family 5, P1 at four different ages during the 14-year interval. N, nasal; T, temporal visual fields; F, family.

creased but far less so at 236 μm. The ORCC was multi-peaked in both eyes. At the perifoveal temporal loci, overall retinal thickness was slightly increased (280 μm). The ONL was reduced in the right eye (14 μm) more than in the left eye (24 μm), with both showing a single-peaked ORCC, and the inner retina was thickened. P1 of family 4 had visual acuity of 20/25 in each eye and each eye retained a multi-peaked ORCC. The right eye foveal thickness was increased at 266 μm, and there were cystic macular changes with an apparent operculum suggesting an evolving macular hole. Foveal thickness in the left eye was far greater at 420 μm with cystic spaces. Perifoveal temporal loci had generally thinned retina in both eyes (144 and 164 μm, respectively), a reduced ONL to 16 to 18 μm with single-peaked ORCC and thinned inner retinal LRP components.

In two further patients (not shown), family 9, P1 and family 5, P1 (Table 1), both with visual acuity of 20/25 or better, cross-sectional images showed normal foveal architecture and thickness, but there was thinned retina at the perifoveal temporal locus with reduced ONL.

DISCUSSION

The Mutant Genes Causing *USH2C* and *USH2A*

Gene and mutation discoveries have defined the *USH2C* and *USH2A* disease subtypes, but the roles of the gene products in the retina are not completely understood. *VLGR1* (or *MASS1*),[29] the *USH2C* gene, encodes a member of the G protein–coupled receptor (GPCR) family of proteins (reviewed in Ref. 30). VLGR1 is the largest cell surface protein known and has similarities to family B GPCRs, specifically a subgroup of large N-terminal seven-transmembrane receptors.[31] The extracellular portion of the VLGR1 protein contains repeated units resembling calcium-exchanger β (calx-β) motifs, which distinguishes it from other GPCRs.[31,32] Both of the *VLGR1* mutations causing *USH2C* in family 1 of this study occur in a calx-β motif.[15] VLGR1 also contains a pentraxin motif[31] that is similar to the LamG domain of the USH2A protein.[33]

Clues to the function of the molecule come from murine studies of *VLGR1* transcript expression, which is highest in the

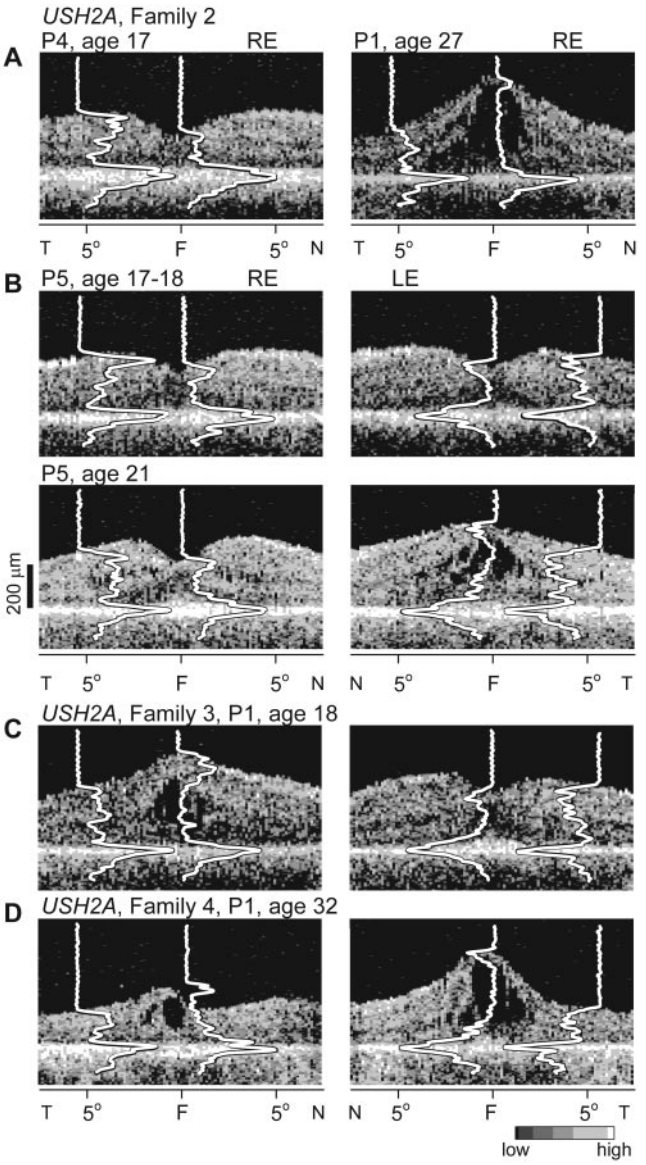

FIGURE 6. Central retinal microstructure in *USH2A*. (**A–B**) Cross-sectional retinal images obtained with OCT from the central 15° of the right eye of family 2, P4 (age 17 years), P1 (age 27), and both eyes of P5 at different ages (ages 17, 18, and 21 years), representing about a 4-year interval. (**C**) Cross-sectional retinal images from both eyes of family 3, P1. (**D**) Cross-sectional retinal images from both eyes of family 4, P1. Images are displayed with the logarithm of reflectivity mapped to a grayscale. LRPs, averaged from 1° sections, are superimposed on the images as in Figure 3. N, nasal; T, temporal retina; F, fovea.

embryonic central nervous system. *VLGR1* transcripts are expressed by neural retinal precursors and by cells destined to become retinal pigment epithelium.[34] The suggestion has thus been made that mutations in *VLGR1* may affect neural development.[34,35] VLGR1 expression continues at low levels in adulthood,[32,34] implying an additional role in maintenance.[34]

The *USH2A* product usherin is thought to be either a cell adhesion molecule or an extracellular matrix protein, based on the presence of laminin and fibronectin domains.[36,37] *USH2A* mRNA expression was originally found to be limited mainly to the retina and cochlea, and cellular expression in rodent and human retina was in the outer nuclear layer.[38] Usherin has also been reported to be widely expressed in the basement membranes of several other rodent and human tissues.[39,40] Usherin is stabilized in basement membranes through its interaction with type IV collagen.[41] In contrast to the high fetal expression of *VLGR1* transcripts, *USH2A* transcripts are expressed at highest levels in the adult neural retina,[42] possibly because the protein functions in cellular homeostasis.[38]

USH2C and *USH2A* Retinal Phenotypes

The retinal degenerative component of all Usher syndromes remains incurable. If gene-based interventions for the retina are in the future for patients with USH, the pathogenesis of the retinopathies must be clarified. Naturally occurring or genetically engineered murine or other models of human diseases[43,44] have become key to the analysis of pathobiology. None of the USH models, however, has a pronounced retinal degenerative component to the phenotype.[2] Understanding the human retinal phenotype is not only a prerequisite for any proposed intervention and for eventual comparison with animal models, but also (and specifically in the case of USH) this information can help bridge the wide gap between gene discovery and disease expression.

USH2C has not previously been studied in detail for retinal phenotype. The three siblings with *USH2C* showed severe peripheral rod and cone dysfunction when first examined in the third and fourth decade of life (within a few years of the first retinal diagnosis).[15] There were no retinal regions with normal rod function, but there were islands of impaired rod function. Rod and cone ERG findings mirrored rod and cone psychophysics. Photoreceptors appear to progress to degeneration in a pattern of rod worse than cone and peripheral worse than central retina. Central retinal architecture can appear normal except when distorted by macular cystic changes. At the perifoveal locus, the outer nuclear layer was reduced in all three patients.

The *USH2A* phenotype showed many similarities to *USH2C* and one notable difference. Some *USH2A* patients had normal rod and cone function and nearly normal outer nuclear layer thickness (at the locus measured). Studying further *USH2C* patients may make this difference disappear. Among the similarities to *USH2C*, all regions showing retinal dysfunction by chromatic perimetry had greater rod than cone losses, and the retina-wide ERG measures were again concordant. As in *USH2C*, the photoreceptor dysfunction in *USH2A* patients appeared to progress to degeneration in a peripheral worse than central pattern. Central retinal structure by OCT was complicated by cystic changes in four of seven patients studied. An *USH2A* disease sequence, based on cross-sectional data and limited longitudinal data, would be as follows: patients could have normal or nearly normal rod and cone function (and structure) in large expanses of retina that progressed at different rates to impaired rod and less impaired cone function, to total loss of rod function and retained, albeit severely reduced, cone function.

How do the present results compare with earlier retinal studies of molecularly-defined *USH2A* patients? We are aware of only two studies.[45,46] In one study of 37 *USH2A* patients,[45] ERGs were reported as not detectable in 35 (age range, 20–59 years) of 37. Two patients (monozygotic twins at age 13) were described as having subnormal rod and cone function. Kinetic perimetry results were listed as ring scotomas and residual central islands. Visual acuity declined with age, and funduscopic hallmarks of retinal degeneration (attenuated vessels and pigmentary retinopathy) increased with age. Another recent work compared *USH2A* with *USH1B* patients by using scores of functional vision.[46] Results of certain studies of ungenotyped USH2 patients are worthy of mention in relation to the present results. The kinetic fields in our patients resembled those illustrated in an earlier study of visual field progression in

retinal degenerations that included USH2 patients (pattern III, 10/24 USH2 patients).[47] Data reduction in other studies of kinetic perimetry in USH2 prevents comparison.[48,49] Previous histopathologic studies of USH2 patients showed many of the features observed in our noninvasive studies of *USH2C* and *USH2A*; foveal macular cystic change, retained perifoveal laminar architecture but reduced outer nuclear layer thickness; the presence of rods and cones, but shortened outer segments in the more central retina; and residual cones but no rods in more peripheral regions.[50,51]

In the recent USH literature, the term phenotypic variability is mentioned in different contexts. Certain genes found to cause USH1 also cause nonsyndromic deafness (reviewed in Ref. 2). *USH2A* mutation has been associated with nonsyndromic RP.[52–55] Concerning the *USH2A* retinal disease spectrum, there is a single report of monozygotic twins with reported differences in visual deficit (as well as differences in hearing and vestibular function). It was suggested that disease severity may not be entirely determined by the *USH2A* gene mutation but may be complicated by other factors.[56] We found major differences in retinal disease severity at the age of 17 years in the dizygotic twins of family 2 and this would add further support to the contention that there may be important roles for modifier genes and environmental factors in *USH2A*. Although the different severities of retinal disease expression in patients in the present study are interpretable as stages of progression, there was no clear relationship between severity and age. Trying to understand how much of this retinal phenotypic variation is due to the specific *USH2A* mutation and how much to other factors, and which factors, may be useful in the development of therapeutic strategies for this very common form of USH and autosomal recessive RP.[55]

Macular Cystic Lesions in *USH2C* and *USH2A*

Foveal lesions, and specifically cystoid macular edema, are a well-known feature not only of USH but of nonsyndromic retinitis pigmentosa (RP; for example, Refs. 57–59). The incidence of macular edema in RP has been most commonly reported to be between 3% and 20% (for example, Refs. 27,57,60–62). In USH2, it has been estimated that approximately 8% of patients have macular edema; greater percentages have been noted in USH1 patients.[58,63] In the *USH2C* and *USH2A* patients, we studied with OCT, there were cystic macular abnormalities in 6 of 10 patients. Serial data documented progression to macular cystic change over a period of years in a patient from each molecular subtype. Although the OCT features of cystic maculopathy in many different retinopathies have been well-documented (for example, Ref. 64), there are very few reports of OCT in patients with RP[27,28,64] and no reports in USH.

USH2C and *USH2A* patients had the expected OCT findings of major increases in foveal thickness in some eyes, but there could also be more subtle changes. Of interest, the latter occurred in the contralateral eyes of those with large hyporeflective lesions (for example, family 1, P6, RE; family 2, P5, RE; and family 3, P1, LE) suggesting the macular changes were a bilateral process with asymmetry. Serial data showed that there could be relatively small degrees of foveal thickening that anticipated overt macular cystic change by years (for example, family 2, P5, LE). The horizontal extent of the abnormality was detectable at the perifoveal temporal locus in some eyes with foveal thickening. There was overall retinal thickening or normal thickness despite outer nuclear layer thinning. Inner nuclear layer thickening was sometimes prominent (for example, family 1, P6, LE at many ages; family 2, P5, LE at age 21; and family 3, P1, RE). The patients we studied with cystic macular changes had visual acuities of 20/30 or better despite different dimensions of foveal lesions. This is consistent with an earlier study in RP which reported no relationship between visual acuity and foveal thickness, unlike in diabetic macular edema. A statistically significant relationship between the width of the lesions and acuity was found.[27] The width of cystic abnormality was not quantified in the present work. A foveal structural detail for correlation with visual acuity may be the vitread ORCC component associated with photoreceptor IS/OS.[20,22,23,25] This OCT feature was present in the USH2 patients of this study.

The basis of macular edema in USH or nonsyndromic RP is poorly understood. The site of the breakdown of the blood–retinal barrier in RP has been investigated clinically with a number of techniques and variously considered as either at the retinal pigment epithelium or the perifoveal capillary plexus or both.[62,65,66] A histopathologic study of eyes with RP led to the conclusion that the main site of permeability was the retinal vasculature.[67] It is unknown whether the USHs have a specific abnormality in regulation of blood–retinal barrier permeability or there is some shared mechanism with RP and other retinal diseases, such as release of growth factors during retinal degeneration and altered vascular permeability.[59,68–70]

Histamine is among the soluble factors suspected to be mediators of blood–retinal barrier dysfunction in diabetes.[68,71,72] It is thus of interest that there was an unexpected and dramatic reduction of longstanding macular cystic change in a *USH2C* patient who was taking oral antihistamines (H1 receptor antagonists). Experimental and pilot human data in diabetes support an effect on blood–retinal barrier permeability of an H1 receptor antagonist.[73,74] The reduction of macular cystic abnormality in our single case does not justify therapeutic recommendations, but warrants further study. If antihistamines could improve macular structure at doses usually recommended for allergic symptoms, then it may be worth considering as a useful primary or adjuvant therapy or after rebound of macular edema after carbonic anhydrase inhibitor use in USH or RP.[75–77]

Acknowledgments

The authors thank Andy Cheung, John Chico, Vaibhav Bhuva, Alexander Pantelyat, Yijun Huang, Daniel Marks, Michael Pianta, Alyson Walsh, Boram Kim, Paul Schied, David Hanna, Laurie Seltzer, Leigh Gardner, Jean Andorf and Jessica Emmons for help with the study.

References

1. Petit C. Usher syndrome: from genetics to pathogenesis. *Annu Rev Genomics Hum Genet*. 2001;2:271–297.
2. Ahmed ZM, Riazuddin S, Riazuddin S, Wilcox ER. The molecular genetics of Usher syndrome. *Clin Genet*. 2003;63:431–444.
3. Keats BJB, Savas S. Genetic heterogeneity in Usher syndrome. *Am J Med Genet.* 2004;130:13–16.
4. Hope CI, Bundey S, Proops D, Fielder AR. Usher syndrome in the city of Birmingham: prevalence and clinical classification. *Br J Ophthalmol*. 1997;81:46–53.
5. Rosenberg T, Haim M, Hauch A-M, Parving A. The prevalence of Usher syndrome and other retinal dystrophy-hearing impairment associations. *Clin Genet*. 1997;51:314–321.
6. van Aarem A, Pinckers AJLG, Kimberling WJ, Huygen PLM, Bleeker-Wagemakers EM, Cremers CWRJ. Stable and progressive hearing loss in type 2A Usher's syndrome. *Ann Otol Rhinol Laryngol*. 1996;105:962–967.
7. Wagenaar M, van Aarem A, Huygen P, Pieke-Dahl S, Kimberling W, Cremers C. Hearing impairment related to age in Usher syndrome types 1B and 2A. *Arch Otolaryngol Head Neck Surg*. 1999;125:441–445.
8. Sankila EM, Pakarinen L, Kaariainen H, et al. Assignment of an Usher syndrome type III (USH3) gene to chromosome 3q. *Hum Mol Genet*. 1995;4:93–98.

9. Kimberling WJ, Weston MD, Moller C, et al. Gene mapping of Usher syndrome type IIa: localization of the gene to a 2.1-cM segment on chromosome 1q41. *Am J Hum Genet*. 1995;56:216–223.
10. Pieke-Dahl S, Kimberling WJ, Gorin MB, et al. Genetic heterogeneity of Usher syndrome type II. *J Med Genet*. 1993;30:843–848.
11. Pieke-Dahl S, van Aarem A, Dobin A, Cremers CWRJ, Kimberling WJ. Genetic heterogeneity of Usher syndrome type II in a Dutch population. *J Med Genet*. 1996;33:753–757.
12. Hmani M, Ghorbel A, Boulila-Elgaied A, et al. A novel locus for Usher syndrome type II, USH2B, maps to chromosome 3 at p23-24.2. *Eur J Hum Genet*. 1999;7:363–367.
13. Ouyang XM, Yam D, Hejtmancik JF, et al. Mutational spectrum in Usher syndrome type II. *Clin Genet*. 2004;65:288–293.
14. Pieke-Dahl S, Moller CG, Kelley PM, et al. Genetic heterogeneity of Usher syndrome type II: localisation to chromosome 5q. *J Med Genet*. 2000;37:256–262.
15. Weston MD, Luijendijk MW, Humphrey KD, Moller C, Kimberling WJ. Mutations in the *VLGR1* gene implicate G-protein signaling in the pathogenesis of Usher syndrome type II. *Am J Hum Genet*. 2004;74:357–366.
16. Jacobson SG, Voigt WJ, Parel JM, et al. Automated light- and dark-adapted perimetry for evaluating retinitis pigmentosa. *Ophthalmology*. 1986;93:1604–1611.
17. Jacobson SG, Yagasaki K, Feuer WJ, Roman AJ. Interocular asymmetry of visual function in heterozygotes of X-linked retinitis pigmentosa. *Exp Eye Res*. 1989;48:679–691.
18. Jacobson SG, Cideciyan AV, Huang Y, et al. Retinal degenerations with truncation mutations in the cone-rod homeobox (*CRX*) gene. *Invest Ophthalmol Vis Sci*. 1998;39:2417–2426.
19. Aleman TS, Cideciyan AV, Volpe NJ, Stevanin G, Brice A, Jacobson SG. Spinocerebellar ataxia type 7 (*SCA7*) shows a cone-rod dystrophy phenotype. *Exp Eye Res*. 2002;74:737–745.
20. Jacobson SG, Cideciyan AV, Aleman TS, et al. *Crumbs homolog* 1 (*CRB1*) mutations result in a thick human retina with abnormal lamination. *Hum Mol Genet*. 2003;12:1073–1078.
21. Jacobson SG, Sumaroka A, Aleman TS, et al. Nuclear receptor *NR2E3* gene mutations distort human retinal laminar architecture and cause an unusual degeneration. *Hum Mol Genet*. 2004;13:1893–1902.
22. Huang Y, Cideciyan AV, Papastergiou GI, et al. Relation of optical coherence tomography retinal images to microanatomy in normal and retinal degeneration chickens. *Invest Ophthalmol Vis Sci*. 1998;39:2405–2416.
23. Huang Y, Cideciyan AV, Aleman TS, et al. Optical coherence tomography (OCT) abnormalities in rhodopsin mutant transgenic swine with retinal degeneration. *Exp Eye Res*. 2000;70:247–251.
24. Jacobson SG, Cideciyan AV, Iannaccone A, et al. Disease expression of *RP1* mutations causing autosomal dominant retinitis pigmentosa. *Invest Ophthalmol Vis Sci*. 2000;41:1898–1908.
25. Pianta MJ, Aleman TS, Cideciyan AV, et al. In vivo micropathology of Best macular dystrophy with optical coherence tomography. *Exp Eye Res*. 2003;76:203–211.
26. Curcio CA, Sloan KR, Kalina RE, Hendrickson AE. Human photoreceptor topography. *J Comp Neurol*. 1990;292:497–523.
27. Hirakawa H, Iijima H, Gohdo T, Tsukahara S. Optical coherence tomography of cystoid macular edema associated with retinitis pigmentosa. *Am J Ophthalmol*. 1999;128:185–191.
28. Apushkin MA, Fishman GA, Janowicz MJ. Monitoring cystoid macular edema by optical coherence tomography in patients with retinitis pigmentosa. *Ophthalmology*. 2004;111:1899–1904.
29. Skradski SL, Clark AM, Jiang H, et al. A novel gene causing a mendelian audiogenic mouse epilepsy. *Neuron*. 2001;31:537–544.
30. Bockaert J, Pin JP. Molecular tinkering of G protein-coupled receptors: an evolutionary success. *EMBO J*. 1999;18:1723–1729.
31. Foord SM, Jupe S, Holbrook J. Bioinformatics and type II G-protein-coupled receptors. *Biochem Soc Trans*. 2002;30:473–479.
32. Nikkila H, McMillan DR, Nunez BS, Pascoe L, Curnow KM, White PC. Sequence similarities between a novel putative G protein-coupled receptor and Na+/Ca2+ exchangers define a cation binding domain. *Mol Endocrinol*. 2000;14:1351–1364.
33. Beckmann G, Hanke J, Bork P, Reich JG. Merging extracellular domains: fold prediction for laminin G-like and amino-terminal thrombospondin-like modules based on homology to pentraxins. *J Mol Biol*. 1998;275:725–730.
34. McMillan DR, Kayes-Wandover KM, Richardson JA, White PC. Very large G protein-coupled receptor-1, the largest known cell surface protein, is highly expressed in the developing central nervous system. *J Biol Chem*. 2002;277:785–792.
35. McMillan DR, White PC. Loss of the transmembrane and cytoplasmic domains of the very large G-protein-coupled receptor-1 (VLGR1 or Mass1) causes audiogenic seizures in mice. *Mol Cell Neurosci*. 2004;26:322–329.
36. Eudy JD, Weston MD, Yao S, et al. Mutation of a gene encoding a protein with extracellular matrix motifs in Usher syndrome type IIa. *Science*. 1998;280:1753–1757.
37. Weston MD, Eudy JD, Fujita S, et al. Genomic structure and identification of novel mutations in usherin, the gene responsible for Usher syndrome type IIa. *Am J Hum Genet*. 2000;66:1199–1210.
38. Huang D, Eudy JD, Uzvolgyi E, et al. Identification of the mouse and rat orthologs of the gene mutated in Usher syndrome type IIA and the cellular source of USH2A mRNA in retina, a target tissue of the disease. *Genomics*. 2002;80:195–203.
39. Bhattacharya G, Miller C, Kimberling WJ, Jablonski MM, Cosgrove D. Localization and expression of usherin: a novel basement membrane protein defective in people with Usher's syndrome type IIa. *Hear Res*. 2002;163:1–11.
40. Pearsall N, Bhattacharya G, Wisecarver J, Adams J, Cosgrove D, Kimberling W. Usherin expression is highly conserved in mouse and human tissues. *Hear Res*. 2002;174:55–63.
41. Bhattacharya G, Kalluri R, Orten DJ, Kimberling WJ, Cosgrove D. A domain-specific usherin/collagen IV interaction may be required for stable integration into the basement membrane superstructure. *J Cell Sci*. 2004;117:233–242.
42. van Wijk E, Pennings RJ, te Brinke H, et al. Identification of 51 novel exons of the *Usher syndrome type* 2A (*USH2A*) gene that encode multiple conserved functional domains and that are mutated in patients with Usher syndrome type II. *Am J Hum Genet*. 2004;74:738–744.
43. Rattner A, Sun H, Nathans J. Molecular genetics of human retinal disease. *Annu Rev Genet*. 1999;33:89–131.
44. Pacione LR, Szego MJ, Ikeda S, Nishina PM, McInnes RR. Progress toward understanding the genetic and biochemical mechanisms of inherited photoreceptor degenerations. *Annu Rev Neurosci*. 2003;26:657–700.
45. van Aarem A, Wagenaar M, Pinckers AJLG, et al. Ophthalmologic findings in Usher syndrome type 2A. *Ophthalmic Genet*. 1995;16:151–158.
46. Pennings RJ, Huygen PL, Orten DJ, et al. Evaluation of visual impairment in Usher syndrome 1b and Usher syndrome 2a. *Acta Ophthalmol Scand*. 2004;82:131–139.
47. Grover S, Fishman GA, Brown J Jr. Patterns of visual field progression in patients with retinitis pigmentosa. *Ophthalmology*. 1998;105:1069–1075.
48. Edwards A, Fishman GA, Anderson RJ, Grover S, Derlacki DJ. Visual acuity and visual field impairment in Usher syndrome. *Arch Ophthalmol*. 1998;116:165–168.
49. Iannaccone A, Kritchevsky SB, Ciccarelli ML, et al. Kinetics of visual field loss in Usher syndrome type II. *Invest Ophthalmol Vis Sci*. 2004;45:784–792.
50. Hunter DG, Fishman GA, Mehta RS, Kretzer FL. Abnormal sperm and photoreceptor axonemes in Usher's syndrome. *Arch Ophthalmol*. 1986;104:385–389.
51. Berson EL, Adamian M. Ultrastructural findings in an autopsy eye from a patient with Usher's syndrome type II. *Am J Ophthalmol*. 1992;114:748–757.
52. Rivolta C, Sweklo EA, Berson EL, Dryja TP. Missense mutation in the *USH2A* gene: association with recessive retinitis pigmentosa without hearing loss. *Am J Hum Genet*. 2000;66:1975–1978.
53. Bernal S, Ayuso C, Antinolo G, et al. Mutations in *USH2A* in Spanish patients with autosomal recessive retinitis pigmentosa: high prevalence and phenotypic variation. *J Med Genet*. 2003;40:E8.

54. Aller E, Najera C, Millan JM, et al. Genetic analysis of 2299delG and C759F mutations (*USH2A*) in patients with visual and/or auditory impairments. *Eur J Hum Genet*. 2004;12:407–410.
55. Seyedahmadi BJ, Rivolta C, Keene JA, Berson EL, Dryja TP. Comprehensive screening of the *USH2A* gene in Usher syndrome type II and non-syndromic recessive retinitis pigmentosa. *Exp Eye Res*. 2004;79:167–173.
56. Liu XZ, Hope C, Liang CY, et al. A mutation (231delG) in the Usher syndrome type IIA gene: high prevalence and phenotypic variation. *Am J Hum Genet*. 1999;64:1221–1225.
57. Fishman GA, Maggiano JM, Fishman M. Foveal lesions seen in retinitis pigmentosa. *Arch Ophthalmol*. 1977;95:1993–1996.
58. Fishman GA, Anderson RJ, Lam BL, Derlacki DJ. Prevalence of foveal lesions in type 1 and type 2 Usher's syndrome. *Arch Ophthalmol*. 1995;113:770–773.
59. Heckenlively JR, Jordan BL, Aptsiauri N. Association of antiretinal antibodies and cystoid macular edema in patients with retinitis pigmentosa. *Am J Ophthalmol*. 1999;127:565–573.
60. Fetkenhour CL, Choromokos E, Weinstein J, Shoch D. Cystoid macular edema in retinitis pigmentosa. *Trans Am Acad Ophthalmol Otolaryngol*. 1977;83:515–521.
61. Heckenlively JR. Clinical findings in retinitis pigmentosa. *Retinitis Pigmentosa.* Heckenlively JR, ed. Philadelphia: JB Lippincott; 1988;81–85.
62. Tranos PG, Wickremasinghe SS, Stangos NT, Topouzis F, Tsinopoulos I, Pavesio CE. Macular edema. *Surv Ophthalmol*. 2004;49:470–490.
63. Piazza L, Fishman GA, Farber M, Derlacki D, Anderson RJ. Visual acuity loss in patients with Usher's syndrome. *Arch Ophthalmol*. 1986;104:1336–1339.
64. Schuman JS, Puliafito CA, Fujimoto JG. *Optical Coherence Tomography of Ocular Diseases*. Thorofare, NJ: Slack; 2004.
65. Cunha-Vaz JG, Travassos A. Breakdown of the blood-retinal barriers and cystoid macular edema. *Surv Ophthalmol*. 1984;28:485–492.
66. Kuchle M, Nguyen NX, Martus P, Freissler K, Schalnus R. Aqueous flare in retinitis pigmentosa. *Graefes Arch Clin Exp Ophthalmol*. 1998;236:426–433.
67. Vinores SA, Kuchle M, Derevjanik NL, et al. Blood-retinal barrier breakdown in retinitis pigmentosa: light and electron microscopic immunolocalization. *Histol Histopathol*. 1995;10:913–923.
68. Antonetti DA, Lieth E, Barber AJ, Gardner TW. Molecular mechanisms of vascular permeability in diabetic retinopathy. *Semin Ophthalmol*. 1999;14:240–248.
69. Kent D, Vinores SA, Campochiaro PA. Macular oedema: the role of soluble mediators. *Br J Ophthalmol*. 2000;84:542–545.
70. Antcliff RJ, Marshall J. The pathogenesis of edema in diabetic maculopathy. *Semin Ophthalmol*. 1999;14:223–232.
71. Enea NA, Hollis TM, Kern JA, Gardner TW. Histamine H1 receptors mediate increased blood-retinal barrier permeability in experimental diabetes. *Arch Ophthalmol*. 1989;107:270–274.
72. Gardner TW, Lesher T, Khin S, Vu C, Barber AJ, Brennan WA Jr. Histamine reduces ZO-1 tight-junction protein expression in cultured retinal microvascular endothelial cells. *Biochem J*. 1996;320:717–721.
73. Hollis TM, Sill HW, Butler C, Campos MJ, Gardner TW. Astemizole reduces blood-retinal barrier leakage in experimental diabetes. *J Diabetes Complications*. 1992;6:230–235.
74. Gardner TW, Eller AW, Friberg TR, D'Antonio JA, Hollis TM. Antihistamines reduce blood-retinal barrier permeability in type I (insulin-dependent) diabetic patients with nonproliferative retinopathy: a pilot study. *Retina*. 1995;15:134–140.
75. Cox SN, Hay E, Bird AC. Treatment of chronic macular edema with acetazolamide. *Arch Ophthalmol*. 1988;106:1190–1195.
76. Fishman GA, Gilbert LD, Fiscella RG, Kimura AE, Jampol LM. Acetazolamide for treatment of chronic macular edema in retinitis pigmentosa. *Arch Ophthalmol*. 1989;107:1445–1452.
77. Fishman GA, Glenn AM, Gilbert LD. Rebound of macular edema with continued use of methazolamide in patients with retinitis pigmentosa. *Arch Ophthalmol*. 1993;111:1640–1646.